PNAS RESEARCH ARTICLE | NEUROSCIENCE

Multiple forms of working memory emerge from synapse–astrocyte interactions in a neuron–glia network model

Maurizio De Pittà[a,b,c,d,1] and Nicolas Brunel[e,f]

Edited by Terrence Sejnowski, Salk Institute for Biological Studies, La Jolla, CA; received May 10, 2022; accepted August 11, 2022

Persistent activity in populations of neurons, time-varying activity across a neural population, or activity-silent mechanisms carried out by hidden internal states of the neural population have been proposed as different mechanisms of working memory (WM). Whether these mechanisms could be mutually exclusive or occur in the same neuronal circuit remains, however, elusive, and so do their biophysical underpinnings. While WM is traditionally regarded to depend purely on neuronal mechanisms, cortical networks also include astrocytes that can modulate neural activity. We propose and investigate a network model that includes both neurons and glia and show that glia–synapse interactions can lead to multiple stable states of synaptic transmission. Depending on parameters, these interactions can lead in turn to distinct patterns of network activity that can serve as substrates for WM.

neuron–glial networks | working memory | gliotransmission | spiking neuron and astrocyte models

Significance

The biophysical underpinnings of working memory are of paramount interest in modern neuroscience. Working memory could be encoded by diverse patterns of neural activity, ranging from persistent firing of neuronal populations to more dynamic patterns of network activity. Silent mechanisms whereby working memory is maintained by synaptic variables have also been suggested. Multiple models exist for these mechanisms but only consider neurons, ignoring glia. We propose that glia could underpin working memory, introducing models of cortical neuron–glial networks where synapse–glia signaling could account for firing and silent working memory encoding. Our theoretical arguments can explain emerging accounts of the variegated nature of working memory encoding and the possible contribution of glia to it.

The neural basis of working memory (WM) remains a subject of debate. A large body of evidence supports a role for sustained neural activity in prefrontal and other cortices, possibly supported by attractor dynamics in recurrently connected circuits (1). In this view, neurons hold sensory information beyond the presentation of a sensory-relevant cue by their persistent firing activity (PA). However, competing evidence suggests that WM could also be accounted for by dynamically varying activity patterns and activity-silent representations (2).

There is a growing debate on whether different mechanisms of WM could coexist within the same brain region (3), and the underpinning cellular substrate for their coexistence remains elusive (2). Activity-dependent synaptic facilitation has emerged in recent years as an appealing candidate mechanism for this coexistence (4, 5). On the one hand, it bestows cortical networks with slow time scales (from hundreds of milliseconds to minutes) that might help stabilize PA (4, 6). On the other, it can also encode memory by synaptic variables whose dynamics can sustain WM in the absence of PA (5).

Although synaptic facilitation is traditionally regarded as a purely neuronal process, we consider here the possibility that it could also involve glial signaling. Among cortical glial cells, astrocytes are ubiquitous in the neuropil. They are prominently found in proximity of nerve terminals, sensing neural activity and being activated during synaptic transmission. Astrocytes can also modulate synaptic transmission by releasing transmitters—dubbed "gliotransmitters" for their glial origin—like glutamate (7). In particular, gliotransmission may promote synaptic release from excitatory terminals for several seconds, up to minutes, thus potentially contributing to WM processing, akin to short-term synaptic facilitation, but on longer time scales. In agreement with this hypothesis, astrocyte stimulation in mouse primary sensory areas increases neural firing beyond stimulation (8, 9). This phenomenon appears in association with changes of neuronal gain by higher concentrations of extracellular glutamate, possibly due to the enhanced release of this neurotransmitter by gliotransmission (8). In this fashion, gliotransmission would mediate a positive feedback on neuronal activity that could also be relevant for WM processing (6).

Results

Neuronal and Synaptic Correlates of WM Induced by Gliotransmission. To investigate the possibility that astrocyte-mediated gliotransmission could be an active player in WM, we started by analyzing a minimal neuron–glial circuit (Fig. 1*A*) of a single integrate-and-fire neuron stimulated by N synapses. A fraction f of those synapses are shared with an astrocyte, leading to interactions in both directions (Fig. 1*B*). Incoming action potentials (APs) trigger synaptic release (r), which occurs stochastically: $r = 1$, with probability u, and 0 otherwise (Fig. 1*C*). We also introduce an integrate-and-fire

Author affiliations: [a]Krembil Research Institute, University Health Network, Toronto, ON, M5T 0S8, Canada; [b]Temerty Faculty of Medicine, Department of Physiology, University of Toronto, Toronto, ON, M5S 1A8, Canada; [c]Division of Mathematical Modeling with Multidisciplinary Applications, Basque Center for Applied Mathematics, 48009 Bilbao, Spain; [d]Faculty of Medicine, University of the Basque Country, 48940 Leioa, Spain; [e]Department of Neurobiology, Duke University, Durham, NC 27710; and [f]Department of Physics, Duke University, Durham, NC 27710

Author contributions: M.D.P. and N.B. designed research; M.D.P. performed research; M.D.P. and N.B. analyzed data; and M.D.P. and N.B. wrote the paper.

The authors declare no competing interest.

This article is a PNAS Direct Submission.

[1]To whom correspondence may be addressed. Email: maurizio.depitta@uhnresearch.ca.

This article contains supporting information online at https://www.pnas.org/lookup/suppl/doi:10.1073/pnas.2207912119/-/DCSupplemental.

Published October 18, 2022.

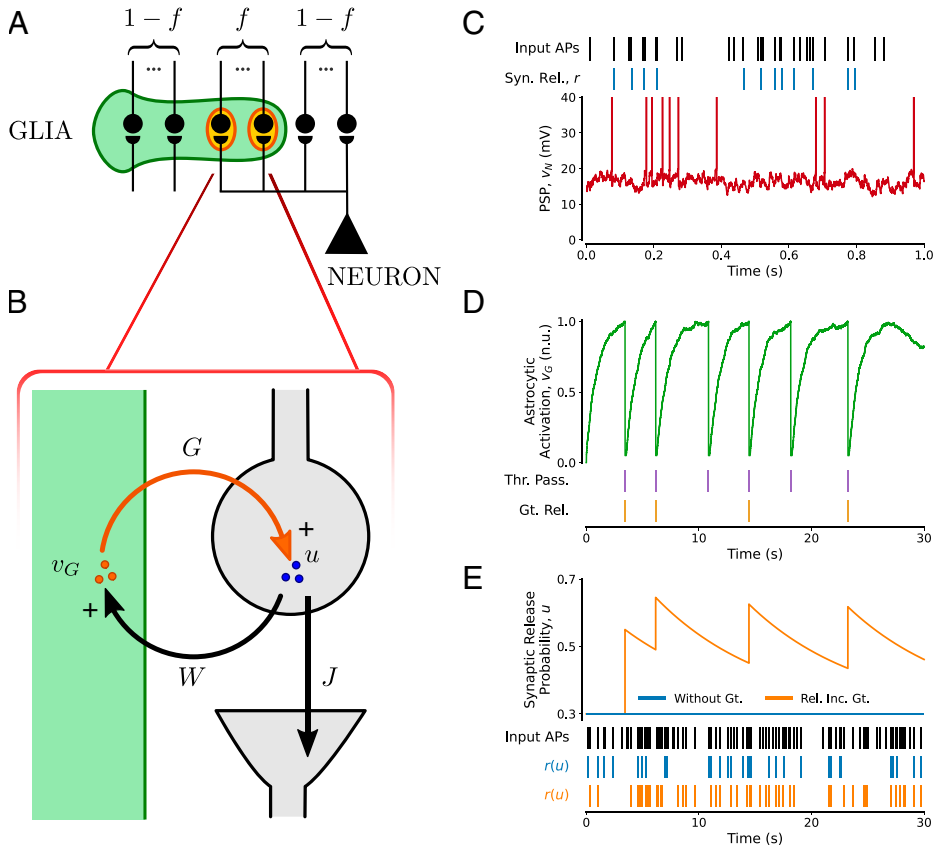

Fig. 1. Minimal neuron–glial circuit. (*A*) Schematics of a single neuron–astrocyte domain, where a fraction f of the synapses are shared by the neuron with the astrocyte. (*B*) Synapse–astrocyte positive feedback loop. Neurotransmitter release r at a presynaptic terminal, occurring with instantaneous probability u, can depolarize both the postsynaptic neuron (by an amount J) and the astrocyte (by W). Astrocyte activation can trigger glutamate release from the astrocyte which, in turn, can lead to an increase in release probability u described by a parameter G. (*C*) Incoming APs at a sample synapse (black raster) trigger stochastic neurotransmitter release (blue raster). The summed synaptic input from $N = 1{,}000$ excitatory synapses drives fluctuations in the membrane potential (v_N) of a leaky integrate-and-fire neuron (red traces), leading to irregular firing (vertical red bars). (*D*) The shared synapses also stimulate the astrocyte whose activation (v_G) is equivalently described by a leaky integrate-and-fire formalism (green trace). Each calcium spike (purple vertical lines) triggers stochastic glutamate (Gt.) release from the astrocyte (yellow vertical lines). (*E*) The instantaneous neurotransmitter release probability from a synapse modulated by astrocytic glutamate (from *D*) (orange trace) is shown together with the release probability from the same synapse in the absence of gliotransmission (blue line). Bottom rasters exemplify how these two scenarios result in different transmission of a train of APs (black raster). Parameters are as in *SI Appendix*, Table S1.

formalism to describe astrocyte activation (v_G) in terms of slow build-up (by W per incoming AP) and fast release of intracellular calcium mediating gliotransmitter release (*Materials and Methods*). Since gliotransmitter release only occurs beyond some calcium threshold and is short-lived with respect to the triggering calcium increases (*SI Appendix*), its timing can be approximated by the timing of intracellular calcium elevations beyond the release threshold. Specifically, we posit that when $v_G = 1$, a calcium spike occurs, triggering glutamate release from the astrocyte with some probability (Fig. 1*D*). Each gliotransmitter release event (GRE), in turn, transiently increases glutamate release probability at those synapses shared between the astrocyte and the neuron (Fig. 1*E*). In agreement with experimental observations (7), this increase decays slowly, with a time scale $\tau_G > 5\,\mathrm{s}$, to the value of release probability attained by the synapses in the absence of gliotransmission (*SI Appendix*).

In the absence of the astrocyte, this minimal circuit is memoryless—the neuronal firing rate only depends on the current inputs, and while an increase in the input rate of presynaptic APs (ν) can increase the neuron's firing rate, this rapidly goes back to baseline after the original input is restored (Fig. 2*A*). In the presence of gliotransmission, the neuronal response to an input can change dramatically, with two possible scenarios. In Fig. 2*B*, gliotransmission is triggered by stimulating the $(1-f)N$ synapses that are not shared with the neuron, while the stimulation rate of the neuron remains constant. In this fashion, gliotransmission occurs only during the stimulus presentation (yellow marks coinciding with the green square pulse in Fig. 2*B*, *Top*), yet it promotes a slow-decaying increase of neurotransmitter release at synapses shared between the neuron and the astrocyte (orange trace). This increases the net synaptic drive to the neuron, resulting in a transient increase of its firing activity that decays over time scales of the order of τ_G (Fig. 2*B*, bottom raster).

A ramping activity can be obtained when gliotransmission is triggered by synapses that also stimulate the neuron (Fig. 2*C*). In this case, the positive feedback of gliotransmission on synaptic stimulation can promote astrocytic glutamate release beyond the cue's presentation and, in turn, keep higher levels of synaptic release in a self-sustained manner. PA may also emerge following the cue for sufficiently strong astrocytic activation, even though presynaptic stimulation recovers to precue rates. PA is generated thanks to the emergence of bistability in the rate of gliotransmitter release (ν_G), as evinced by considering the steady-state solutions for such release rate. The rate ν_G is the inverse of the mean time between two consecutive GREs in which astrocyte activity reaches the threshold for gliotransmitter release (v_t^G) from the reset value (v_r^G) attained immediately after the first GRE. It can be expressed as a function of the time-averaged synaptic release probability $U = \langle u \rangle_{\Delta T}$ at shared synapses in a time interval $\Delta T \to \infty$ by the mean ($\mu_G(U) = fNWU\nu\tau_G$) and SD of the synaptic input to the astrocyte ($\sigma_G(U) = \sqrt{W\mu_G}$), namely,

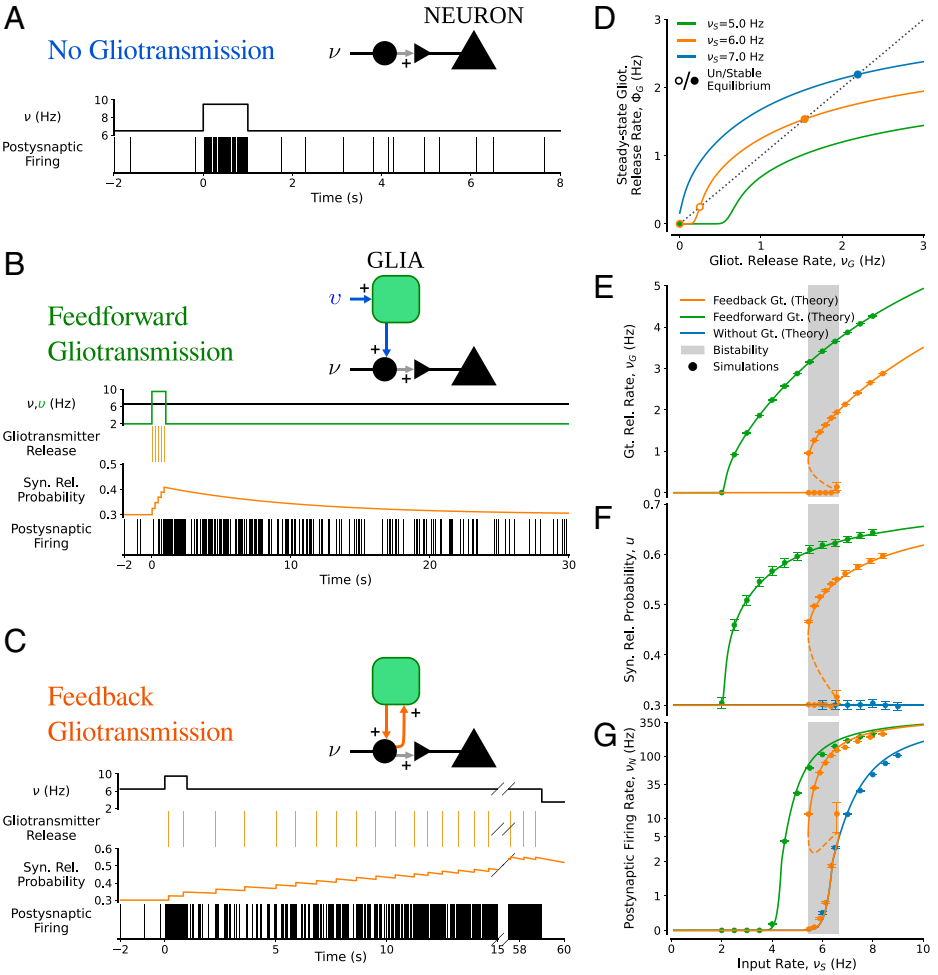

Fig. 2. WM in the minimal neuron–glial circuit. (*A*) In the absence of gliotransmission, the circuit is memoryless, and neuronal firing (raster) quickly returns to baseline right after the presentation of a square-pulse input current (*Top*; for $0 \leq t < 1$ s). (*B*) The astrocyte can be independently selectively stimulated (green square pulse) to trigger gliotransmitter release (yellow raster). This results in the transient increase of synaptic release probability (orange trace) associated with a long-lasting temporary increase of postsynaptic firing (black raster). (*C*) Postsynaptic firing can ramp up, and eventually turn persistent, when gliotransmission is stimulated by the same synapses that it modulates (yellow raster). When this occurs, synaptic release is bistable, leading to two stable postsynaptic firing rates, one low, the other high (black raster, for $t < 0$ and $t > 15$ s). (*D*–*G*) Local stability analysis of the minimal neuron–astrocyte circuit. (*D*) Graphical solutions of the steady-state rates of gliotransmitter release: one or two stable rates exist depending on the rate of synaptic stimulation (ν_S). Mapping such rates for all ν_S values provides the bifurcations diagrams for (*E*) the rate of gliotransmitter release from the astrocyte, (*F*) the synaptic release probability, and (*G*) the firing rate of the postsynaptic neuron. The sigmoid-shaped bifurcation diagrams in the presence of feedback gliotransmission hallmark the emergence of bistability with hysteresis (orange curves and data points). Theoretical curves were constructed by numerical continuation of mean-field equations (*SI Appendix*, Eqs. **S17**–**S19**). Data points and error bars indicate mean ± SD across 20 synapses in $n = 20$ simulations. Solid/dashed curves indicate stable/unstable equilibria. Parameters are as in *SI Appendix*, Table S1.

$$\nu_G = \left(\tau_G^r + \int_{\frac{v_r^G - \mu_G(U)}{\sigma_G(U)}}^{\frac{v_t^G - \mu_G(U)}{\sigma_G(U)}} \mathrm{d}z \Psi_G(z) \right)^{-1} = \Phi_G\left(\mu_G(U), \sigma_G(U)\right), \quad [1]$$

where $\Psi_G(z) = \tau_G \sqrt{\pi} \exp(z^2)(1 + \mathrm{erf}(z))$, and τ_G^r represents the absolute refractory period for gliotransmitter release (10, 11) (*SI Appendix*). When gliotransmission does not modulate the synaptic input to the astrocyte, $\Phi_G\left(\mu_G, \sigma_G\right)$ in Eq. **1** provides an explicit function to estimate the average steady-state rate of gliotransmitter release at given (constant) U values. In this case, Φ_G coincides with the classic solution of the first passage-time problem of a leaky integrate-and-fire neuron with a white noise input current (11, 12). On the other hand, when the synaptic input to the astrocyte is modulated by gliotransmission, U becomes a function of ν_G (*SI Appendix*, Eq. **8**), and the solutions of Eq. **1** can be graphically found by the intersections of the straight line of slope unity with the curve given by the right-hand side of Eq. **1** as a function of $U(\nu_G)$. In this scenario, besides the trivial solution for the intersection at $\nu_G \sim 0$, two other intersections may exist for $\nu_G > 0$, depending on the rate of synaptic stimulation (ν_S) of which the one at higher ν_G, is stable, while the other is not. The minimal neuron–glial circuit is thus bistable since two distinct steady-state rates of gliotransmitter release exist for the same synaptic stimulation: a very low rate when synaptic stimulation is not sufficient to promote gliotransmission and a higher rate of a few release events per second when gliotransmission is promoted by synaptic stimulation.

Gliotransmission Brings Forth Bistable Synaptic Release. Analysis of the bifurcation diagrams for $\nu_G(\nu_S)$ in Fig. 2*E* allows appreciating how bistability (gray shaded) only exists in the presence of positive feedback mediated by release-increasing gliotransmission on the astrocyte's synaptic input. Moreover, the sigmoid shape of the orange diagram in Fig. 2*E* associated with feedback gliotransmission reveals the existence of hysteresis, that is, the dependence of gliotransmitter release on the astrocyte's activation history. For such release to occur steadily, not only the rate of

synaptic stimulation must be in the gray-shaded range, but also the astrocyte's activity must be above the dashed line in Fig. 2*E* that represents the unstable fixed point. Only in this case can the increase in synaptic release ensuing from gliotransmission promote further gliotransmitter release from the astrocyte in a self-sustained fashion that can outlast the original synaptic stimulation.

A corollary of this reasoning is that in the presence of positive feedback by gliotransmission and for appropriate rates of synaptic stimulation, steady-state synaptic release in the minimal neuron–glial circuit may be either low, for very low gliotransmitter release, or high for sustained gliotransmitter release (Fig. 2*F*). These different levels of synaptic release, in turn, result in different postsynaptic firing rates (Fig. 2*G*). Thus, the postsynaptic neuron that would be silent or fire sporadically for low stimulation rates in the absence of gliotransmission ($\nu_S < 6.5$ Hz) instead fires in the same conditions yet with sustained gliotransmitter release from the astrocyte. Hence, when an input pushes synaptic release from the low attractor to the high one, like in the simulation in Fig. 2*C*, the neuron's activation is also expected to ramp up after the cue presentation, reminiscent of experimental observations in delay periods of delayed response tasks (3, 13, 14). The ramping-up ultimately ends with neuronal firing stabilizing at a constant steady-state rate of PA. The ensuing firing is higher than that otherwise attained by the neuron in the low synaptic release attractor, until a sufficiently long decrease in external input resets it to baseline. In this model, sustained activity can be highly irregular, with a coefficient of variation of the neuron's interspike interval distribution that can be higher than baseline and also be above one (*SI Appendix*, Fig. S1), in agreement with the observed irregularity of PA in delayed response tasks (15). In addition, bistability of synaptic release and neuronal firing by feedback gliotransmission in the minimal circuit occurs robustly for a broad range of neuronal and astrocytic parameters (*SI Appendix*, Fig. S2).

WM in Neuron–Glial Networks. The next question we ask is whether bistability could also emerge in large cortical neuron–glial networks. To answer this question, we considered a network of 4,000 excitatory (E) and 1,000 inhibitory (I) randomly connected neurons (16) that interact with 4,000 astrocytes (G). Denoting $\epsilon = 1{,}000/4{,}000$ as the E: I neuron ratio, each neuron receives exactly C_E excitatory synapses and ϵC_E inhibitory ones from other neurons in the network. Motivated by experimental data, we consider the case where all these recurrent excitatory and inhibitory synapses stimulate astrocytes, but only excitatory ones are modulated by gliotransmission (7). In this regard, we assume that recurrent synapses can randomly connect with equal probability to any astrocyte in the network, so that each astrocyte is stimulated by K_E excitatory synapses and ϵK_E inhibitory ones (*SI Appendix*). The contribution of excitatory and inhibitory synapses to neuronal depolarization is J and $-g_J J$, whereas both synapse types contribute to astrocyte activation by W (*Materials and Methods*).

Analysis of the asynchronous state of the ensuing EI + G network confirms the possibility of bistability by the positive feedback of gliotransmission on recurrent excitatory connections. This can be seen considering the solutions of the system of implicit equations for the network's average rates of neuronal firing (ν_N) and gliotransmitter release (ν_G) (*SI Appendix*)

$$\nu_\alpha = \Phi_\alpha\left(\mu_\alpha(\nu_N, \nu_G), \sigma_\alpha(\nu_N, \nu_G)\right), \qquad [2]$$

where $\Phi_\alpha(\mu_\alpha, \sigma_\alpha)$ $(\alpha = N, G)$ is in the form of Eq. **1** and yields the firing rate of a cell in population α receiving noisy inputs of mean μ_α with SD σ_α. Eq. **2** generalizes those for balanced neuronal networks introduced by Amit and Brunel (17) to neuron–glial networks, where the mean inputs to neurons and glia and the corresponding amplitude of fluctuations read (*SI Appendix*)

$$\mu_N = C_E J\left((U - g_J\epsilon)\nu_N + \nu_X\right)\tau_N \quad \sigma_N = \sqrt{C_E \mu_N}, \quad [3]$$

$$\mu_G = K_E W(U + \epsilon)\nu_N \tau_G \quad \sigma_G = \sqrt{K_E \mu_G}. \quad [4]$$

In the above equations, it is convenient to express the rate of stimulation of external inputs to the network as $\nu_X = \rho\nu_\theta$, where ν_θ is the rate of stimulation needed for a neuron to fire in the absence of recurrent inputs (16). Then, as illustrated by the orange curve in Fig. 3*A*, two stable equilibria, reflecting up and down asynchronous states, at high and low firing rates, respectively, can coexist separated by an unstable equilibrium depending on the values of two parameters: the strength of the network's recurrent inhibitory connections (g_J) and the strength of afferent excitatory stimulation to the neurons (ρ). While bistability can exist in purely neuronal unstructured EI networks (16, 18), the presence of glia–synapse interactions dramatically expands the parameter region in which bistability occurs. A comparison of the orange bifurcation diagrams of the EI + G network as functions of g_J (Fig. 3) and ρ (Fig. 3*C*) with those of the same EI network without glia (green and blue diagrams, respectively) reveals that bistability in the EI + G network could emerge for regimes of strong recurrent inhibition and strong external excitation that, in the absence of gliotransmission, could account for only one stable asynchronous state instead. Such bistability could also be found in the presence of moderate noise levels, mimicking putative gliotransmitter release ensuing from spontaneous calcium dynamics in astrocytes (19) (red diagrams). Moreover, it could be found for arbitrarily large values of recurrent inhibition and external excitation, in stark contrast with the mere EI network (Fig. 3*D*). In the latter, external excitation and recurrent inhibition exert opposite effects on the average network's firing: the former increases it, whereas the latter decreases it. In the presence of glia, however, because both excitatory and inhibitory connections promote the gliotransmitter release, these two opposite effects can compete, resulting in close but distinctly higher (lower) firing rates besides those otherwise attained by the network in the absence of gliotransmission, with strong recurrent inhibition (strong external excitation). The range for bistability in the $g_J - \rho$ plane ultimately depends on the relative scaling of the contribution of inhibitory synapses vs. excitatory ones to glial activation (*SI Appendix*, Fig. S3).

A simulation of a randomly connected EI + G network (Fig. 3*E*) allows appreciating how bistability emerges in the inhibition-dominated regime by feedback gliotransmission, providing a mechanism for WM (bottom orange trace) in a network that would be otherwise memoryless without astrocytes (blue trace). Here a short high-frequency step increase of afferent stimulation can push the network from the DOWN to the UP state, triggering PA (Fig. 3*E*, *Bottom*, orange vs. blue traces). However, because the increase of excitatory drive mediated by gliotransmission competes with the strong inhibition, PA firing rates differ by just a few Hz from the DOWN state. At the same time, ongoing gliotransmission changes the internal state of excitatory synapses, providing a latent mechanism for WM by facilitation of synaptic release probability (Fig. 3*E*, *Middle*, orange trace). This also holds for more silent versions of WM achieved by lower spontaneous activity and allows reactivating the cue's memory by weaker nonspecific inputs presented to the network, as long as gliotransmission-mediated synaptic facilitation is high enough (*SI Appendix*, Figs. S4 and S5).

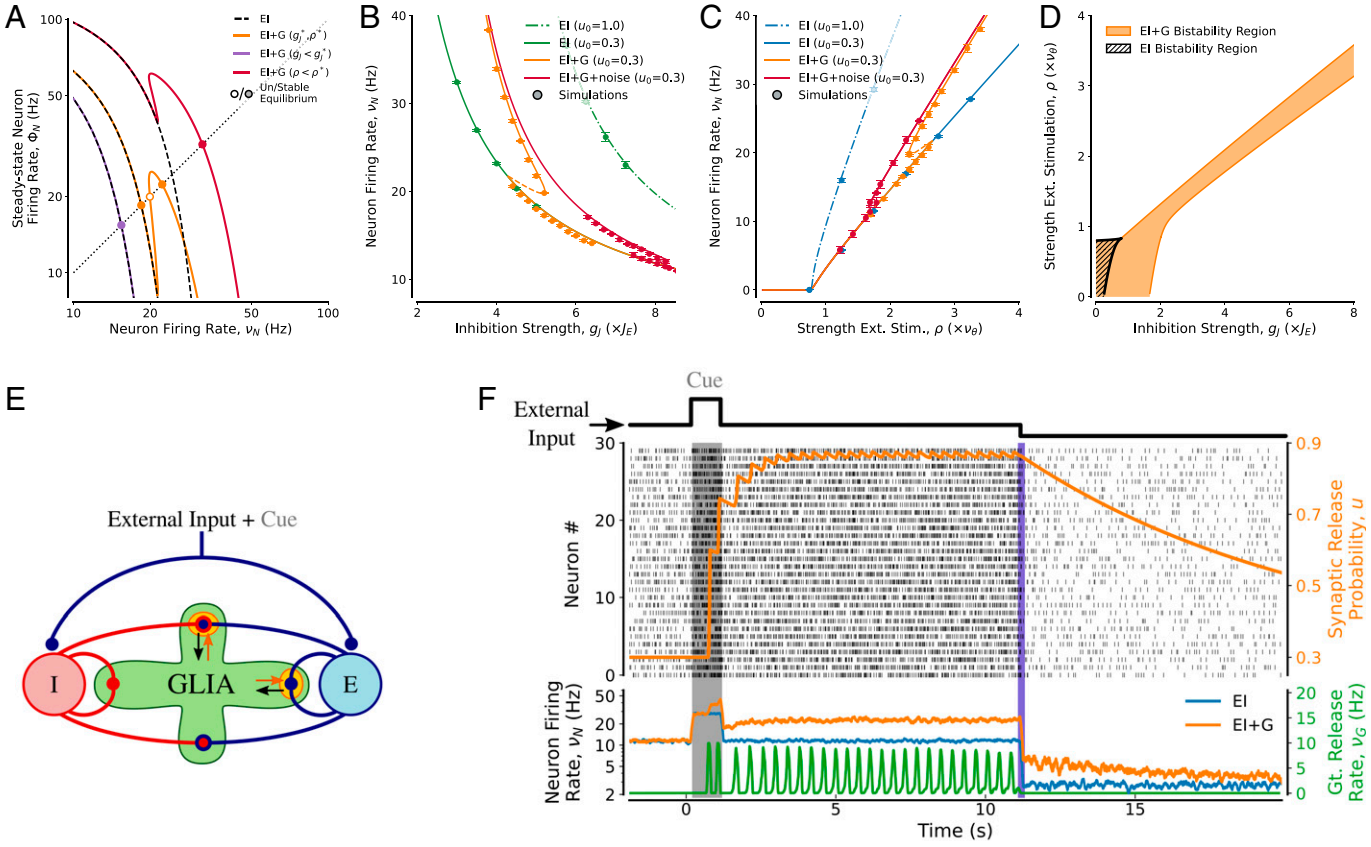

Fig. 3. WM in neuron–glial networks. (*A–D*) Bistability in a randomly connected EI + G network. (*A*) Graphic solution of the self-consistency equations for the asynchronous state(s) (SI Appendix, Eq. **S47**) reveals the possibility of coexistence of two stable equilibria separated by an unstable one (orange curve) in a range of values of g_J and ρ ($g_J^* = 5$, $\rho^* = 2.2$). While stronger inhibition prevents the onset of persistent gliotransmission, resulting in low firing rates ($g_J = 6$, purple curve), stronger external stimuli promote gliotransmission, leading to a distinct firing rate of the asynchronous state ($\rho = 2.7$, red curve). Such bistability of the asynchronous state is exclusively by gliotransmission since only one equilibrium is found solving the self-consistency equations for the mere neuronal (EI) network (black dashed lines), regardless of the scenario under consideration. Firing rates of the network's asynchronous states (*B*) as a function of recurrent inhibition and (*C*) as a function of the external excitatory input. The orange bifurcation diagram for the EI + G network with basal synaptic release probability $u_0 = 0.3$ always lies between the diagrams of the EI network without gliotransmission for the same value of u_0 (solid blue and green curves) and for deterministic synaptic release ($u_0 = 1$, dash-dotted curves). In the case of the EI + G network, there exists an intermediate range of both g_J and ρ values for two distinct asynchronous states: a low-rate one, similar to the one that exists in the EI network in the absence of gliotransmission, and a higher-rate one, resulting from ongoing, persistent gliotransmitter release from the astrocyte network. (*D*) Comparison between the bistability regions of the neuron-only EI network (hashed area) and the bistability region in the EI + G network (orange area). In the EI + G network, the bistability region is composed of two parts: 1) for $\rho < 0.8$, a region that extends bistability in EI network toward higher inhibitory drive and 2) for $\rho > 0.8$, a stripe that extends into the inhibition-dominated region ($g_J > 2$). This shape is a consequence of our assumption that both excitatory and inhibitory synapses stimulate astrocytes, but only excitatory ones are strengthened by gliotransmission. In this fashion, as inhibition grows, it comes to compete with release-increasing gliotransmission at excitatory connections: only when excitation reinforced by gliotransmission wins over inhibition does bistability emerge. Simulations (circles) agree with analytical results. Data and error bars are mean ± SD for $n = 5$ different network realizations simulated for 20 s. (*E* and *F*) Persistent activity emerging from gliotransmission-mediated bistability in a neuron–glia network. (*E*) Random neuron–glia (EI + G) network model (*Materials and Methods*). (*F*) The EI + G network is stimulated by a brief square pulse (cue with rate of ∼25 Hz) for $0 \leq t < 1$ s (dark shading). Without gliotransmission, neuronal firing quickly returns to baseline after cue presentation (blue trace). In the presence of gliotransmission, the cue promotes a persistent increases of synaptic excitation (u, top orange trace), resulting in PA. Black dots indicate spike rasters of a representative subset of 30 excitatory neurons. The purple bar marks a reduction of afferent excitation, leading to a reduction in neuronal activity. Parameters are as in *SI Appendix*, Table S2.

Synaptic–Astrocyte Connectivity Can Account for Multi-Item WM Encoding. The topology of synapse–astrocyte interactions is an additional important factor in shaping network dynamics. Different synaptic ensembles modulated by distinct astrocytes could promote discrete domains of excitation and inhibition (20), resulting in heterogeneous active neuronal populations. Consider the scenario in Fig. 4*A* where the astrocytes in the EI + G network belong to two disjoint populations that split the neurons into distinct subnetworks whose recurrent connections are modulated by distinct astrocytes. Without astrocytes, the selective stimulation of a subnetwork transiently promotes the firing of neurons in that subnetwork that also leads to a transient surge of feedback inhibition to the rest of the network, suppressing the firing of unstimulated neurons (blue traces in the dark gray shades) (Fig. 4*B*), as in standard attractor neural networks with strong recurrent inhibition (21). Moreover, after cue presentation, no PA is observed as the network is dominated by inhibition. With the addition of astrocytes, the stimulated subnetwork can instead turn persistently active by the selective stimulation of the associated astrocyte population. In this way, the ensuing increase of recurrent excitation promoted by gliotransmission remains spatially confined within the subnetwork (top u orange trace) (Fig. 4*B*). The whole network can also be switched to another memory state, by a sufficiently strong stimulation of the second subnetwork, which leads to suppression of the first (gray shade at $t = 4$ s) (Fig. 4*B*). Moreover, thanks to the slow time scale τ_G of decay of the modulation of synaptic excitation by gliotransmission, it is possible to reactivate individual memories by ∼30% weaker stimuli to individual subnetworks (light gray shades) (Fig. 4*B*). In this fashion, different domains of gliotransmission from distinct astrocyte populations, promote clustered network activity. Each cluster encodes a separate WM item and emerges as a neuronal

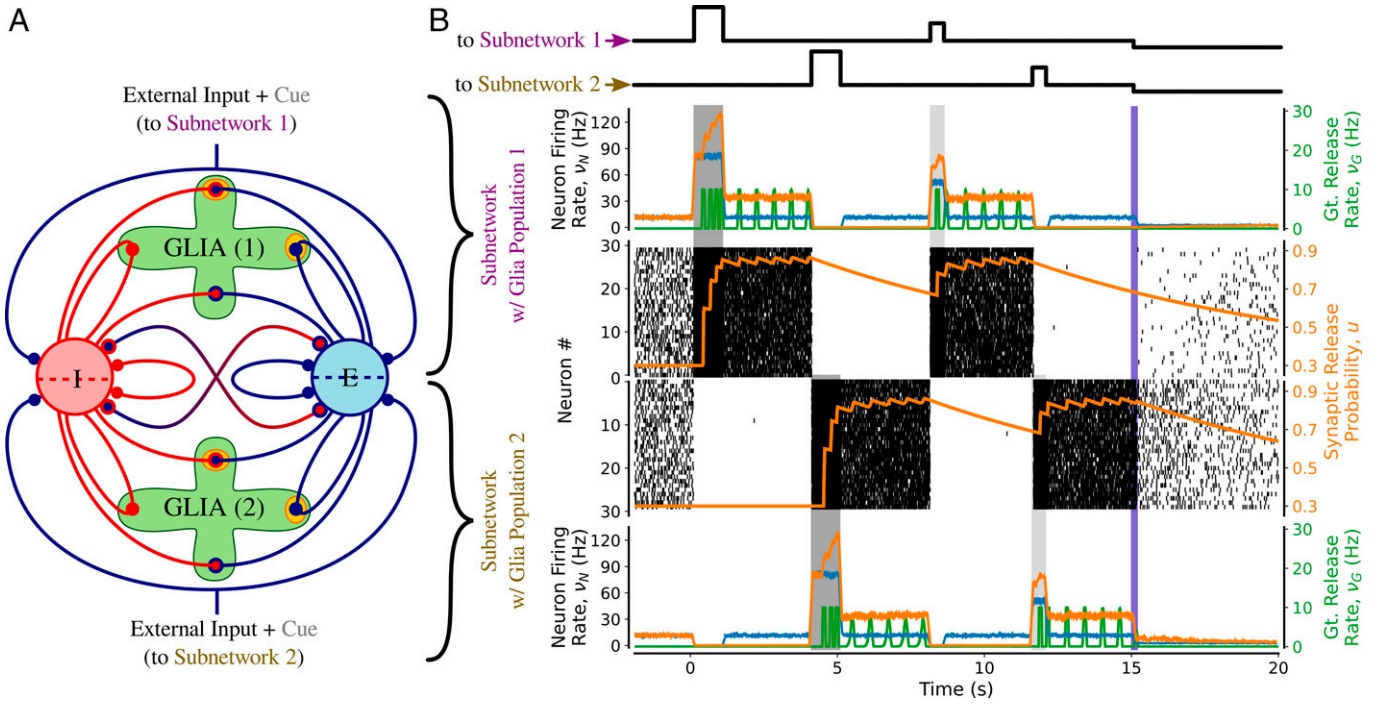

Fig. 4. Multistability in structured EI + G networks encoding two distinct memories. (*A*) Structured EI + G network model. The network of Fig. 3*E* is separated in two subnetworks (1, 2) of equal E, I and G cell numbers. Recurrent synapses in each subnetwork are modulated by distinct astrocyte populations (*Materials and Methods*). (*B*) A random subset of 50% of neurons in subnetwork 1 is stimulated by a high-frequency (∼60 Hz) cue, promoting PA in subnetwork 1, while suppressing most of subnetwork 2's activity thanks to recurrent inhibition. At $t = 4$ s, the cue is fed to subnetwork 2, making it persistently active, while suppressing activity in subnetwork 1. Individual memories can be reactivated by weaker stimulations (30 Hz) of single subnetworks, occurring within a temporal window of about $\tau_G = 10$ s. Parameters are as in *SI Appendix*, Table S2.

population that is kept persistently active by spatially segregated astrocyte activation and the associated gliotransmission modulating synaptic release. These observations also hold for moderate noise levels of gliotransmission (*SI Appendix*, Fig. S6), mimicking spontaneous and stochastic glial activity (*SI Appendix*).

Discussion

The cellular and circuit bases of WM have been the subject of debate for decades. The traditional view is that WM maintenance depends on the stationary persistence of neural activity patterns representing specific memory items. However, this view has been challenged by emerging evidence that PA does not always accompany WM maintenance but could instead wax and wane as a function of the current task relevance of memoranda (13, 22). These observations spurred the idea that WM might not reside entirely in the spiking activity but could also be maintained by nonspiking, activity-silent mechanisms, like short-term facilitation (5). While traditionally regarded to be exclusively mediated by synaptic mechanisms, we propose that mechanisms of synaptic facilitation underpinning WM could be mediated by gliotransmission from astrocytes (23, 24).

Combining numerical simulations of biophysically realistic neuron–glial circuits with analytical calculations, we show how astrocytic gliotransmission could sustain different WM activity patterns observed experimentally, at the level of both individual neurons and large cortical networks. In our models, dynamical patterns of WM can be generated by the slowly decaying facilitation of synaptic weights by gliotransmission—up to tens of seconds slower than the decay of traditional short-term synaptic facilitation (7)—and can encompass ramping-up, persistent, and ramping-down neuronal firing patterns. These patterns could occur network-wide or be confined to portions of the network under the influence of specific astrocyte populations, suggesting that cortical networks could exploit distinct astrocyte populations to encode multiple WM items.

Multi-item WM is not a prerogative of neuron–glial networks. It can be generated by purely neuronal networks in which connectivity has been structured by Hebbian plasticity, with both static synapses (25) and dynamic synapses (5). Here we propose a scenario in which synaptic connectivity is left unstructured but in which distinct ensembles of potentiated synapses encoding distinct memoranda emerge through different domains of gliotransmitter-mediated synaptic facilitation under the influence of different astrocyte populations.

In our network model consisting of two astrocyte populations, triggering PA in the subnetwork associated with one astrocyte population suppresses memory-related firing in the remainder of the network under the influence of the other astrocyte population. However, in the portion of the network where activity is suppressed, a silent memory encoding persists, thanks to the slowly vanishing synaptic facilitation mediated by gliotransmission. Presenting a noisy input to the silent subnetwork before the decay of gliotransmission-mediated facilitation can indeed restore PA in that subnetwork while switching WM encoding in the active subnetwork to activity-silent. This behavior supports recent accounts that activity-based vs. activity-silent forms of memory maintenance, which have traditionally been regarded as mutually exclusive, could rather coexist in the same brain region (3). We suggest that heterogeneous domains of gliotransmission ensuing from different astrocyte populations (26, 27) could be the biophysical substrate for the coexistence of such different WM forms.

Optogenetic and chemogenetic approaches adopted to study astrocytes' influence on other memory forms could be used to monitor and manipulate the molecular pathways underpinning gliotransmission selectively and test our hypotheses (28, 29). In this regard, optogenetics imaging of astrocytic calcium activity

in WM tasks supports our simulations revealing the temporally precise delayed onset of the astrocyte's activity with neuronal firing at WM onset, maintenance, and recall (30). Likewise, genetic suppression of synaptically activated astrocytic calcium signaling correlates with reduced cognitive performance in classic WM experiments like the Y maze–based spontaneous alternation task (31) and the T maze–based delayed nonmatching-to-place task (23). While other mechanisms of astrocytic origin rather than gliotransmission could underpin such experimental observations, compelling evidence exists that agrees with our model predictions insofar as WM encoding could originate from gliotransmission-mediated modulations of the network's excitatory vs. inhibitory balance (23).

It will be important to characterize better experimentally the anatomy of the connections between cortical synapses, and astrocytes (32), given our observation that multistability could emerge from neuron–glia networks in which astrocytes define specific neuronal clusters. Clustered neuronal activity could emerge from the heterogeneous astrocyte arrangement across the brain (27), within brain regions, and in specific circuits (33). Such a scenario is in agreement with recent experimental and theoretical studies that identify the anatomy of individual astrocytes (34, 35), as well as their possible arrangement into syncytial networks (36, 37), as key aspects in the emergence of neuronal firing ensembles in cognitive-related tasks (32).

On the other hand, the same astrocyte population could also dynamically exert multiple neuromodulatory actions on distinct neurons by a combination of different calcium-dependent pathways (38, 39) and synaptic activity requirements (40, 41). This aligns with the growing recognition that sensory input dynamics could dictate the spatial extent and temporal dynamics of astrocytic calcium signals (39, 40, 42) and thus, potentially, of gliotransmission (7, 32, 43). In turn, modeling arguments suggest this as a biophysical substrate to relay information of multiple memoranda by minimally overlapping spatial domains of calcium-dependent gliotransmission (44). It remains, however, unclear to what extent the number of possible memoranda that could be stored by neuron–glial networks depends on the reciprocal arrangement of astrocytes with respect to neurons and synaptic elements (44).

The modulations of intrasynaptic calcium by extrasynaptically located presynaptic receptors bound by gliotransmitters could exert varied effects on synaptic transmission besides increasing the release probability. For instance, they could interfere with mechanisms of short-term plasticity, speeding up the refilling process of synaptic vesicles (45), thus enabling sustained release at the synaptic terminals for extended periods, as required by our theory (e.g., Fig. 3*F*). At the same time, independent theoretical investigations suggest that the modulation of short-term plasticity by gliotransmission, in combination with the network's noise, could also stabilize (or not) WM depending on the ongoing activity, ultimately controlling WM duration by modulating its mechanisms of onset and termination (46). Thus, including short-term synaptic plasticity in our neuron–glial models is expected to enrich the activity requirements for different WM forms emerging by gliotransmission.

We focus here on the well-documented homosynaptic scenario of regulation of synaptic release by gliotransmission, where the same synapses that stimulate an astrocyte are also modulated by gliotransmission from it. Nonetheless, we predict our theory to also hold for gliotransmitter-mediated increases of postsynaptic efficacy and heterosynaptic modes of gliotransmission (7), as long as they mediate a positive feedback loop in the circuit that can be self-sustained. On the other hand, gliotransmission could also nonlinearly depend on the history of activation of interacting astrocytic domains (41, 47), which could be accounted for by nonlinear extensions of the integrate-and-fire astrocyte model, and the addition of astrocyte–astrocyte interactions in the EI + G network model.

While we have restricted ourselves to multistability between several asynchronous states, other, more dynamic scenarios for WM maintenance could also be dependent on gliotransmission. Dynamical regulations of neuronal gain could alter cortical tuning properties of neuronal ensembles with possible repercussions on dynamic WM encoding (13, 22, 48). There is also emerging evidence that astrocytic gliotransmission could modulate cognitive-relevant brain rhythms (9, 40, 49), which might play a role in WM maintenance (50, 51). These intriguing possibilities require future efforts to characterize the variety of possible neuron–glial networks' spatiotemporal dynamics.

Materials and Methods

Single Neuron–Astrocyte Domain. We consider a minimal neuron–glial circuit of a neuron (N) and an astrocyte (G). There are $N = 1{,}000$ identical synapses in total feeding into the circuit, which are independently stimulated by trains of Poisson-distributed APs, modeled by Dirac delta functions, i.e., $s_i(t) = \sum_k \delta(t - t_i^k)$ for the ith synapse. A fraction f of these synapses is shared by the neuron and the astrocyte. Those synapses stimulate both cells and are modulated by gliotransmission from the astrocyte. The remaining $(1 - f)N$ synapses stimulate instead only the astrocyte, in the scenario of feedforward gliotransmission (Fig. 2*B*), or only the neuron, in the case of feedback gliotransmission (Fig. 2*C*).

Glutamate release from synaptic terminals is described by a Bernoulli process: when an AP reaches a presynaptic terminal, release occurs with probability u, with each release occurring independently from all other ones. We thus define a train of synaptic releases $\tilde{s}_i(t) = \sum_k r_i^k \delta(t - t_i^k)$, where r_i^k are independent Bernoulli random variables describing release occurring with probability $u(t_i^k)$ following the kth spike at synapse i. Each glutamate release instantaneously depolarizes the neuron by J, while increasing astrocytic activation by W. Neuronal depolarization (v_N) is described by a leaky integrate-and-fire (LIF) formalism, such that

$$\frac{dv_N}{dt} = -\frac{v_N}{\tau_N} + J\sum_j \tilde{s}_j(t), \qquad [5]$$

where τ_N is the characteristic decay time constant for neuronal depolarization. Every time v_N reaches a threshold value v_t^N, the neuron generates an AP, and v_N is reset to v_r^N and subsequently held to this value for a refractory period τ_r^N. We also consider an LIF description for astrocytic activation. This activation can be thought of as being an increasing function of the astrocyte's intracellular Ca^{2+} concentration, which critically regulates gliotransmitter release (*SI Appendix*). Astrocytic Ca^{2+} activity (v_G) is driven by synaptic stimulation $i_G(t)$ according to

$$\frac{dv_G}{dt} = -\frac{v_G}{\tau_G} + i_G(t) \qquad [6]$$

with $i_G(t) = W\sum_j \tilde{s}_j(t)$, and τ_G is a lumped time constant for stimulus integration by astrocytic Ca^{2+} signaling (*SI Appendix*, *Physical Justification of the Leaky Integrate-and-Fire Astrocyte Model*). Because gliotransmitter release only occurs when Ca^{2+} reaches a threshold v_t^G, a GRE is set to occur when $v_G > v_t^G$, following which v_G is reset to and held at baseline v_r^G for a refractory period τ_r^G (*SI Appendix*).

Both astrocytic calcium signaling (42) and gliotransmitter release have a stochastic component (52, 53); therefore, we also consider a stochastic description of GREs. That is, GREs are modeled by independent identically distributed. Bernoulli random variables r_G^k whose value is 1 (release success) with probability u_G, and 0 (release failure) otherwise, for each astrocytic threshold crossing k. The single GRE in this context represents the total release of gliotransmitter per threshold crossing, and it does not account for potentially different mechanisms of gliotransmitter release (19). In this fashion, the sequence of GREs originating from the astrocyte, each occurring at instants t_G^k, is described by $g(t) = \sum_k r_G^k \delta(t - t_G^k)$.

At synapses that are shared with the astrocyte, synaptic release probability u is taken to be modulated by GREs from the astrocyte according to (*SI Appendix*, *Derivation of the Gliotransmission Model*)

$$\frac{du}{dt} = \frac{u_0 - u}{\tau_p} + G(\xi - u)g(t), \qquad [7]$$

where u_0 stands for the (baseline) synaptic release probability in the absence of gliotransmission, G and $\xi > u_0$ control the strength of the positive feedback of gliotransmission on synaptic release, and τ_p is the decay time constant of the increase of synaptic release mediated by gliotransmission.

Neuron–Glial Network. The model network of excitatory and inhibitory neurons originally introduced by Brunel (16) is extended to include astrocytes. The resulting neuron–glial network is composed of $N_G = 4{,}000$ astrocytes (G), together with $N_E = 4{,}000$ excitatory neurons (E) and $N_I = 1{,}000$ inhibitory neurons (I). All neurons (astrocytes) are described by an LIF formalism, with identical membrane time constants τ_N (τ_G) and firing thresholds v_t^N (v_t^G). Neurons in the network are randomly connected such that each neuron receives $C_E = 400$ connections from excitatory neurons and $C_I = 100$ connections from inhibitory neurons. Additionally, all neurons are supposed to be stimulated by C_E excitatory afferents from the same cell population (X) outside the network. Synaptic release from neuron j to i (r_{ij}) is probabilistic at recurrent excitatory connections, with a probability (u_{ij}) that depends on GREs from the astrocytes, as described above. For simplicity, we consider identical postsynaptic potential amplitudes $J > 0$ at excitatory synapses and $-g_J J$ at inhibitory synapses. The external synapses are taken to be stimulated by independent Poisson processes with rate $\nu_X = \rho\nu_\theta$, where $\nu_\theta = v_t^N/(JC_E\tau_N)$ is the external frequency that leads to an average membrane potential equal to the neuronal firing threshold. In this fashion, the external input to the network is modeled by a background noisy current, with mean $\mu_X = C_E J\nu_X\tau_N$ and variance $\sigma_X^2 = J\mu_X$. Denoting by $\tilde{s}_{ij}(t) = \sum_k r_{ij}^k \delta(t - t_j^k)$ the train of synaptic releases from excitatory neuron j, where r_{ij}^k are independent Bernoulli random variables with release probability $u_{ij}(t_j^k)$, and by $s_j^I(t)$ the spike train for inhibitory neuron j, the depolarization v_i^α of the ith neuron in population $\alpha = E, I$ evolves according to

$$\frac{dv_i^\alpha}{dt} = -\frac{v_i^\alpha}{\tau_N} + J\sum_{j\in\mathcal{E}_i}\tilde{s}_{ij}(t) - g_J J\sum_{j\in\mathcal{I}_i} s_j^I(t) + \frac{\mu_X}{\tau_N} + \frac{\sigma_X}{\tau_N}\eta_X(t), \qquad [8]$$

where $\eta_X(t)$ is a temporally uncorrelated normal random variable with mean 0 and variance 1, and $\mathcal{E}_i$ ($\mathcal{I}_i$) denotes the set of all excitatory (inhibitory) synapses impinging onto neuron i.

All synapses, regardless of their type, can depolarize glial cells. This reflects the experimental observation that both glutamatergic (excitatory) and GABAergic (inhibitory) synapses can trigger calcium-dependent gliotransmission (7, 54). We assume that all synapses contribute equally to astrocytic depolarization by W. Moreover, given that the molecular machinery for gliotransmission is found in juxtaposition with synaptic terminals (55), we assume that each excitatory synapse stimulating an astrocyte is also modulated by gliotransmission from the latter. Although gliotransmission has also been documented at inhibitory synapses, we limit our analysis to pathways of release-increasing gliotransmission to excitatory synapses only as the latter accounts for the majority of available evidence supporting gliotransmission (43).

Accordingly, the depolarization v_G^i of the ith astrocyte and the release probabilities of excitatory synapses are described by the set of coupled differential equations

$$\frac{dv_i^G}{dt} = -\frac{v_i^G}{\tau_G} + W\sum_{(j,l)\in\mathcal{A}_i^E}\tilde{s}_{jl}(t) + W\sum_{(j,l)\in\mathcal{A}_i^I} s_l^I(t), \qquad [9]$$

$$\frac{du_{jl}}{dt} = \frac{u_0 - u_{jl}}{\tau_p} + G(\xi - u_{jl})g_i(t) \qquad \text{for all } (j,l)\in\mathcal{A}_i^E, \qquad [10]$$

where g_i is the train of GREs originating from the kth astrocyte, and $\mathcal{A}_i^\alpha$ is the set of all α synapses impinging on astrocyte i. Specifically, we consider different scenarios for connections between recurrent synapses and astrocytes. In the random network of Fig. 3*E* and *F*, each astrocyte picks a random subset $\mathcal{N}_s/N_G$ of synapses, out of a total of $\mathcal{N}_s = (C_E + C_I)(N_E + N_I)$ recurrent synapses. In the EI + G network of Fig. 4 instead, the EI neuron network was partitioned into two subnetworks of equal numbers of neurons $[(N_E + N_I)/2]$ and synapses $(\mathcal{N}_s/2)$. Then, recurrent connections of those subnetworks were assigned to distinct populations of $N_G/2$ astrocytes.

In our neuron–glial networks, the number of neurons per astrocyte is 1.25, and an astrocyte domain can contain between 300 and 600 synapses, depending on whether we consider two distinct astrocyte populations or one population only (Fig. 4). These figures agree with experimental data (56) in mice and are also in line with whole-brain estimations of the neuron-to-glia ratio by isotropic fractionation (*SI Appendix*). Likewise, the fact that only recurrent synapses ($\mathcal{N}_s$ in total) but not external ones ($C_E(N_E + N_I)$ in total) are coupled with astrocytes in our networks accounts for ∼55% of synapses associated with astrocytes, reflecting recent data suggesting that 40 to 80% of cortical synapses are likely astrocyte-regulated (57, 58).

Mathematical Analysis. Mean-field analyses of the minimal neuron–glial circuit (Fig. 2) and the unstructured EI + G network (Fig. 3) were performed along the lines of Amit and Brunel (17). We choose the network's parameters such that the mean firing rate of excitatory neurons equals that of inhibitory cells, $\nu_E = \nu_I = \nu_N$. Details can be found in *SI Appendix*, *Mean Field Analysis*.

Numerical Methods. Simulations and mean field analysis used custom code implemented in C/C++, Python 3+, and the Python-based Brian 2 simulator (59). Numerical integration used either an event-based scheme or the Euler–Maruyama method with time step $dt = 10$ μs. Bifurcation diagrams were generated by MatCont 7.3 in MATLAB (R2017a, MathWorks) (60). Simulations were performed on an Intel Xeon 12-core CPU E5-1660 at 3.30 GHz Linux desktop. The Python classes to reproduce the neuron–glial circuits of this study can be downloaded from GitHub (https://github.com/depitta-lab/eig-classes-pnas-2022) (61).

Data, Materials, and Software Availability. There are no data underlying this work. Code to reproduce the models contained in this study are available from GitHub (https://github.com/depitta-lab/eig-classes-pnas-2022) (61).

ACKNOWLEDGMENTS. We thank Paolo Bonifazi and Yair Lakretz for comments on the manuscript and Marcel Stimberg for technical support on the code to simulate the spiking models. This work was originally funded by a Marie Skłodowksa-Curie International Outgoing Fellowship to M.D.P. (Project 331486 "Neuron-Astro-Nets").

1. C. Constantinidis *et al.*, Persistent spiking activity underlies working memory. *J. Neurosci.* **38**, 7020–7028 (2018).
2. J. Kamiński, U. Rutishauser, Between persistently active and activity-silent frameworks: Novel vistas on the cellular basis of working memory. *Ann. N. Y. Acad. Sci.* **1464**, 64–75 (2020).
3. J. Barbosa *et al.*, Interplay between persistent activity and activity-silent dynamics in the prefrontal cortex underlies serial biases in working memory. *Nat. Neurosci.* **23**, 1016–1024 (2020).
4. O. Barak, M. Tsodyks, Working models of working memory. *Curr. Opin. Neurobiol.* **25**, 20–24 (2014).
5. G. Mongillo, O. Barak, M. Tsodyks, Synaptic theory of working memory. *Science* **319**, 1543–1546 (2008).
6. R. Chaudhuri, I. Fiete, Computational principles of memory. *Nat. Neurosci.* **19**, 394–403 (2016).
7. A. Araque *et al.*, Gliotransmitters travel in time and space. *Neuron* **81**, 728–739 (2014).
8. G. Perea, A. Yang, E. S. Boyden, M. Sur, Optogenetic astrocyte activation modulates response selectivity of visual cortex neurons in vivo. *Nat. Commun.* **5**, 3262 (2014).
9. K. E. Poskanzer, R. Yuste, Astrocytes regulate cortical state switching in vivo. *Proc. Natl. Acad. Sci. U.S.A.* **113**, E2675–E2684 (2016).
10. D. J. Amit, M. Tsodyks, Quantitative study of attractor neural network retrieving at low spike rates. I. Substrate-spikes, rates and neuronal gain. *Network: Comput. Neural Syst* **2**, 259 (1991).
11. A. J. Siegert, On the first passage time probability problem. *Phys. Rev.* **81**, 617 (1951).
12. L. M. Ricciardi, *Diffusion Processes and Related Topics in Biology* (Springer Science & Business Media, 1977), vol. 14.
13. M. G. Stokes, 'Activity-silent' working memory in prefrontal cortex: A dynamic coding framework. *Trends Cogn. Sci.* **19**, 394–405 (2015).
14. H. K. Inagaki, L. Fontolan, S. Romani, K. Svoboda, Discrete attractor dynamics underlies persistent activity in the frontal cortex. *Nature* **566**, 212–217 (2019).
15. A. Compte *et al.*, Temporally irregular mnemonic persistent activity in prefrontal neurons of monkeys during a delayed response task. *J. Neurophysiol.* **90**, 3441–3454 (2003).

16. N. Brunel, Dynamics of sparsely connected networks of excitatory and inhibitory spiking neurons. *J. Comput. Neurosci.* **8**, 183–208 (2000).
17. D. J. Amit, N. Brunel, Model of global spontaneous activity and local structured activity during delay periods in the cerebral cortex. *Cereb. Cortex* **7**, 237–252 (1997).
18. E. M. Tartaglia, N. Brunel, Bistability and up/down state alternations in inhibition-dominated randomly connected networks of LIF neurons. *Sci. Rep.* **7**, 11916 (2017).
19. I. Savtchouk, A. Volterra, Gliotransmission: Beyond black-and-white. *J. Neurosci.* **38**, 14–25 (2018).
20. M. M. Halassa, T. Fellin, H. Takano, J. H. Dong, P. G. Haydon, Synaptic islands defined by the territory of a single astrocyte. *J. Neurosci.* **27**, 6473–6477 (2007).
21. N. Brunel, X. J. Wang, Effects of neuromodulation in a cortical network model of object working memory dominated by recurrent inhibition. *J. Comput. Neurosci.* **11**, 63–85 (2001).
22. M. Lundqvist, P. Herman, E. K. Miller, Working memory: Delay activity, yes! Persistent activity? Maybe not. *J. Neurosci.* **38**, 7013–7019 (2018).
23. S. Mederos *et al.*, GABAergic signaling to astrocytes in the prefrontal cortex sustains goal-directed behaviors. *Nat. Neurosci.* **24**, 82–92 (2021).
24. G. Perea, A. Araque, Astrocytes potentiate transmitter release at single hippocampal synapses. *Science* **317**, 1083–1086 (2007).
25. D. J. Amit, A. Bernacchia, V. Yakovlev, Multiple-object working memory–A model for behavioral performance. *Cereb. Cortex* **13**, 435–443 (2003).
26. O. A. Bayraktar *et al.*, Astrocyte layers in the mammalian cerebral cortex revealed by a single-cell in situ transcriptomic map. *Nat. Neurosci.* **23**, 500–509 (2020).
27. D. Lanjakornsiripan *et al.*, Layer-specific morphological and molecular differences in neocortical astrocytes and their dependence on neuronal layers. *Nat. Commun.* **9**, 1623 (2018).
28. B. S. Khakh, M. V. Sofroniew, Diversity of astrocyte functions and phenotypes in neural circuits. *Nat. Neurosci.* **18**, 942–952 (2015).
29. A. Kol, I. Goshen, The memory orchestra: The role of astrocytes and oligodendrocytes in parallel to neurons. *Curr. Opin. Neurobiol.* **67**, 131–137 (2021).
30. Z. Lin *et al.*, Entrainment of astrocytic and neuronal Ca^{2+} population dynamics during information processing of working memory in mice. *Neurosci. Bull.* **38**, 474–488 (2021).
31. J. Nagai *et al.*, Specific and behaviorally consequential astrocyte G_q GPCR signaling attenuation in vivo with iβARK. *Neuron* **109**, 2256–2274.e9 (2021).
32. M. Santello, N. Toni, A. Volterra, Astrocyte function from information processing to cognition and cognitive impairment. *Nat. Neurosci.* **22**, 154–166 (2019).
33. R. Refaeli *et al.*, Features of hippocampal astrocytic domains and their spatial relation to excitatory and inhibitory neurons. *Glia* **69**, 2378–2390 (2021).
34. L. P. Savtchenko, D. A. Rusakov, Regulation of rhythm genesis by volume-limited, astroglia-like signals in neural networks. *Philos. Trans. R. Soc. Lond. B Biol. Sci.* **369**, 20130614 (2014).
35. J. Schummers, H. Yu, M. Sur, Tuned responses of astrocytes and their influence on hemodynamic signals in the visual cortex. *Science* **320**, 1638–1643 (2008).
36. C. Giaume, C. C. Naus, J. C. Sáez, L. Leybaert, Glial connexins and pannexins in the healthy and diseased brain. *Physiol. Rev.* **101**, 93–145 (2021).
37. G. Dallérac, J. Zapata, N. Rouach, Versatile control of synaptic circuits by astrocytes: Where, when and how? *Nat. Rev. Neurosci.* **19**, 729–743 (2018).
38. T. V. Vaidyanathan, M. Collard, S. Yokoyama, M. E. Reitman, K. E. Poskanzer, Cortical astrocytes independently regulate sleep depth and duration via separate GPCR pathways. *eLife* **10**, e63329 (2021).
39. R. Martín, R. Bajo-Grañeras, R. Moratalla, G. Perea, A. Araque, Circuit-specific signaling in astrocyte-neuron networks in basal ganglia pathways. *Science* **349**, 730–734 (2015).
40. G. Perea *et al.*, Activity-dependent switch of GABAergic inhibition into glutamatergic excitation in astrocyte-neuron networks. *eLife* **5**, e20362 (2016).
41. A. Covelo, A. Araque, Neuronal activity determines distinct gliotransmitter release from a single astrocyte. *eLife* **7**, e32237 (2018).
42. A. Semyanov, C. Henneberger, A. Agarwal, Making sense of astrocytic calcium signals–From acquisition to interpretation. *Nat. Rev. Neurosci.* **21**, 551–564 (2020).
43. M. De Pittà, N. Brunel, A. Volterra, Astrocytes: Orchestrating synaptic plasticity? *Neuroscience* **323**, 43–61 (2015).
44. S. Y. Gordleeva *et al.*, Modelling working memory in spiking neuron network accompanied by astrocytes. *Front. Cell. Neurosci.* **15**, 631485 (2021).
45. J. S. Dittman, A. C. Kreitzer, W. G. Regehr, Interplay between facilitation, depression, and residual calcium at three presynaptic terminals. *J. Neurosci.* **20**, 1374–1385 (2000).
46. S. Becker, A. Nold, T. Tchumatchenko, Modulation of working memory duration by synaptic and astrocytic mechanisms. *PLoS Comput. Biol.* **18**, e1010543.
47. T. M. Pirttimaki, S. D. Hall, H. R. Parri, Sustained neuronal activity generated by glial plasticity. *J. Neurosci.* **31**, 7637–7647 (2011).
48. K. K. Sreenivasan, M. D'Esposito, The what, where and how of delay activity. *Nat. Rev. Neurosci.* **20**, 466–481 (2019).
49. H. S. Lee *et al.*, Astrocytes contribute to gamma oscillations and recognition memory. *Proc. Natl. Acad. Sci. U.S.A.* **111**, E3343–E3352 (2014).
50. E. K. Miller, M. Lundqvist, A. M. Bastos, Working memory 2.0. *Neuron* **100**, 463–475 (2018).
51. M. Lundqvist *et al.*, Gamma and beta bursts underlie working memory. *Neuron* **90**, 152–164 (2016).
52. M. Potokar *et al.*, Astrocytic vesicle mobility in health and disease. *Int. J. Mol. Sci.* **14**, 11238–11258 (2013).
53. D. N. Bowser, B. S. Khakh, Two forms of single-vesicle astrocyte exocytosis imaged with total internal reflection fluorescence microscopy. *Proc. Natl. Acad. Sci. U.S.A.* **104**, 4212–4217 (2007).
54. G. Losi, L. Mariotti, G. Carmignoto, GABAergic interneuron to astrocyte signalling: A neglected form of cell communication in the brain. *Philos. Trans. R. Soc. Lond. B Biol. Sci.* **369**, 20130609 (2014).
55. P. Jourdain *et al.*, Glutamate exocytosis from astrocytes controls synaptic strength. *Nat. Neurosci.* **10**, 331–339 (2007).
56. H. Chai *et al.*, Neural circuit-specialized astrocytes: Transcriptomic, proteomic, morphological, and functional evidence. *Neuron* **95**, 531–549.e9 (2017).
57. L. Abdeladim *et al.*, Multicolor multiscale brain imaging with chromatic multiphoton serial microscopy. *Nat. Commun.* **10**, 1–14 (2019).
58. N. Kasthuri *et al.*, Saturated reconstruction of a volume of neocortex. *Cell* **162**, 648–661 (2015).
59. M. Stimberg, R. Brette, D. F. Goodman, Brian 2, an intuitive and efficient neural simulator. *eLife* **8**, e47314 (2019).
60. A. Dhooge, W. Govaerts, Y. A. Kuznetsov, H. G. E. Meijer, B. Sautois, New features of the software MATCONT for bifurcation analysis of dynamical systems. *Math. Comput. Model. Dyn. Syst.* **14**, 147–175 (2008).
61. M. De Pitta, N. Brunel, Code for "Multiple forms of working memory emerge from synapse-astrocyte interactions in a neuron-glia network model." GitHub. https://github.com/depitta-lab/eig-classes-pnas-2022. Deposited 1 October 2022.